Imaging the First-Order Magnetic Transition in $La_{0.35}Pr_{0.275}Ca_{0.375}MnO_3$

Mark H. Burkhardt,[1,2] M. A. Hossain,[1,*] S. Sarkar,[1] Y.-D. Chuang,[3] A. G. Cruz Gonzalez,[3] A. Doran,[3] A. Scholl,[3] A. T. Young,[3] N. Tahir,[3,4] Y. J. Choi,[5] S.-W. Cheong,[6] H. A. Dürr,[1] and J. Stöhr[1,7]

[1]*Stanford Institute for Materials and Energy Sciences (SIMES), SLAC National Accelerator Laboratory, Menlo Park, California 94025, USA*

[2]*Department of Applied Physics, Stanford University, Stanford, California 94305, USA*

[3]*Advanced Light Source, Lawrence Berkeley National Laboratory, Berkeley, California 94720, USA*

[4]*National Center for Physics, Quaid-e-Azam University Campus, Islamabad, Pakistan*

[5]*Department of Physics and IPAP, Yonsei University, Seoul 120-749, Korea*

[6]*Rutgers Center for Emergent Materials and Department of Physics & Astronomy, Rutgers University, Piscataway, New Jersey 08854, USA*

[7]*Linac Coherent Light Source, SLAC National Accelerator Laboratory, Menlo Park, California 94025, USA*

(Received 21 February 2012; published 5 June 2012)

The nature of the ferromagnetic, charge, orbital, and antiferromagnetic order in $La_{0.35}Pr_{0.275}Ca_{0.375}MnO_3$ on the nano- and microscale was investigated by photoemission electron microscopy (PEEM) and resonant elastic soft x-ray scattering (RSXS). The structure of the ferromagnetic domains around the Curie temperature T_C indicates that they nucleate under a high degree of lattice strain, which is brought about by the charge, orbital, and antiferromagnetic order. The combined temperature-dependent PEEM and RSXS measurements suggest that the lattice distortions associated with charge and orbital order are glassy in nature and that phase separation is driven by the interplay between it and the more itinerant charge carriers associated with ferromagnetic metallic order, even well below T_C.

DOI: 10.1103/PhysRevLett.108.237202 PACS numbers: 75.47.Gk, 61.43.Fs, 71.30.+h, 75.25.Dk

Manganites have been the subject of intense study since the discovery of colossal magnetoresistance (CMR). CMR is so large because multiple electronic phases are present simultaneously in a single material, in a phenomenon known as phase separation [1]. Phase separation arises in part because incompatible phases are close in energy: a small change in composition can turn a material with a ferromagnetic metallic (FM) ground state to one with a charge and orbital ordered and antiferromagnetic insulating (CO/OO/AF) ground state [2]. Local compositional inhomogeneities, however, cannot explain phase separation [3]. The answer instead lies with inhomogeneities associated with electronic order: Jahn-Teller distortions, which are associated with localized electrons either as single polarons or CO/OO/AF, inhibit the formation of the FM phase [4]. This has been seen in $La_{0.7}Ca_{0.3}MnO_3$ and bilayered $La_{2-2x}Sr_{1+2x}Mn_2O_7$, in which there is a weakly first-order phase transition between the paramagnetic insulating (PI) and FM phase [5–7]. In these materials, the single polarons that inhabit the PI phase freeze, become so-called glassy polarons [6,7]. In other compounds, there is CO/OO/AF above T_C, and the phase transition between CO/OO/AF and FM is strongly first order [8]. Our measurements imply that the CO/OO/AF is glassy in nature, so the phase transitions are first order for the same reason in all of these materials.

The $La_{0.625-y}Pr_yCa_{0.375}MnO_3$ series of compounds allows us to study the interplay of the CO/OO/AF and FM phases: its parent compounds are FM, with no long-range CO/OO/AF ($y = 0$) and CO/OO/AF, with no metallic phase ($y = 0.625$). For intermediate values of y, there is a low-temperature FM phase. Above the Curie temperature T_C, there is CO/OO/AF, which electron microscopy has shown coexists with a charge-disordered phase that may be paramagnetic or ferromagnetic [8,9]. There are collective lattice distortions in the CO/OO/AF regions but not in the charge-disordered regions. As discussed in Ref. [9], the lattice distortions do not introduce structural defects into the crystal, so there is not an abrupt interface between the two regions but rather an area of accommodation strain within the charge-disordered regions. At high temperatures, only the PI phase exists. In this Letter, we argue that in $La_{0.35}Pr_{0.275}Ca_{0.375}MnO_3$ (LPCMO), the CO/OO/AF is glassy above T_C, inhibiting the formation of the FM phase. The phase transition to the FM phase is spatially inhomogeneous, with large FM regions and large nonmagnetic regions coexisting. This glassy nature is clearest in the correlation length of the CO/OO/AF regions above T_C; they are much larger on warming from the FM phase, where the charge carriers are itinerant, than they are on cooling from the PI phase, where the charge carriers are localized. Below T_C, we argue that there is a battle between the FM and CO/OO/AF phases, fought in the regions of accommodation strain. This cannot be understood as as system in thermal equilibrium, where one phase would vanquish another, so it appears that phase separation is the direct result of glassy behavior.

We measured the spatial characteristics of the FM and CO/OO/AF phases, employing two x-ray techniques. To measure the FM phase, we used photoemission electron

microscopy (PEEM), which provides images of the FM domains. For the CO/OO/AF phase, we used resonant elastic soft x-ray scattering (RSXS). RSXS probes only regions with superlattice order, and it provides a great deal of information about the electronic phases that it probes [10–12]. A single crystal of LPCMO was grown using the floating zone method. We took the PEEM images at the Advanced Light Source (ALS) in Berkeley, California, at beam line 11.0.1, using the PEEM3 endstation. We performed our RSXS measurements at the ALS beam line 8.0.1, using a four-circle diffractometer.

Figures 1(a) and 1(b) illustrate our experimental techniques. In both cases, we used monochromatic x rays, which were linearly polarized for the RSXS measurements and circularly polarized for the PEEM measurements. Typical RSXS momentum scans are illustrated in Fig. 1(c). As with all of the RSXS data shown here, they were taken at $q = (0\frac{1}{2}0)$ in orthorhombic notation at photon energy 639.25 eV, where the RSXS intensity was highest at 120 K upon warming. Later, we will discuss the intensity and correlation length determined from RSXS. The area under the curve is the RSXS intensity, which is a measure of the order parameter, while the correlation length of the ordered domains is inversely proportional to the width. The sets of data on top were taken at 170 K, above T_C, and those on the bottom were taken at 60 K, below T_C. Clearly, this is a significant thermal hysteresis, both in the amplitude and, at 170 K, the width of the curves.

Figure 1(d) shows two PEEM XMCD images, each taken at the same temperature as the RSXS scans next to it in Fig. 1(c). The XMCD signal is proportional to, $\mathbf{m} \cdot \hat{\mathbf{k}}$ where $\mathbf{m}$ is the sample magnetization and $\mathbf{k}$ is the wave

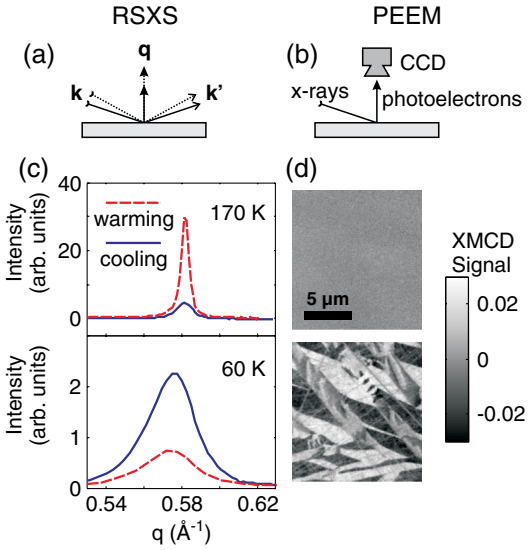

FIG. 1 (color online). (a) The experimental geometry for the RSXS experiments. $\mathbf{k}$ and $\mathbf{k}'$ are the incoming and outgoing photon wave vectors, respectively. (b) Experimental geometry for PEEM. (c) Momentum scans and (d) XMCD images taken at 170 K (top) and 60 K (bottom).

vector of the incoming photons, which come from the left side of the images, making an angle of 30° to the sample surface. The image contrast was generated by use of right and left circularly polarized light and calculating the difference divided by the sum [13]. The FM domains are very large, with the largest approaching 10 μm. As can be seen most clearly in the 48 K image, there are four levels of gray in the image since our sample consists of two twinned crystallographic regions, with corresponding easy magnetization directions.

Figure 2 shows typical PEEM images taken over the accessible temperature range. We took all of the images during the same cooling-warming cycle. In the inset, we show the images around T_C warming, but at a higher contrast than the other images in Fig. 2. There is a thermal hysteresis between ~71 K and 125 K. In the images that show ferromagnetic domains, the domain pattern does not change from image to image except for those taken near T_C. Around T_C, especially between 100 K and 75 K cooling and at 122 K warming, there are two features not visible elsewhere. The first is that the FM domains take the form of mostly alternating stripes rather than the large domains present when $T \ll T_C$. The second is that there are large gray regions, which are not FM, that coexist with large FM regions, so the phase transition temperature is spatially inhomogeneous. To fully explain these phenomena, we need to look at the CO/OO/AF.

We summarize our RSXS measurements in Figs. 3(a)–3(c). The triangles show data taken during traditional warming and cooling scans. We took a third scan where we cooled the sample to 32 K, then warmed to 150 K so that we were on the warming side of the hysteresis. We then performed a cooling scan from that point, and diamonds show those measurements. Each scan resulted in a different value for T_C. Below T_C, there is still superlattice order. There are two striking features: at T_C on warming the scattered intensity and the correlation length reach significantly higher values than at the same temperature on cooling, and the correlation length appears to rise slowly on warming between the temperatures labeled T_C and T_g. As we will discuss below, the glassy nature of the CO/OO/AF is responsible for both.

Figure 3(c) shows the peak q positions that we obtained from our fits of the individual momentum scans. RSXS is sensitive only to electronic order, so the values of q that we measured correspond only to the CO/OO/AF regions of the sample. Above T_C, q is constant because the CO/OO/AF is the only ordered phase present. Once the FM phase takes over, q decreases significantly and continues to decrease as the temperature is lowered. To facilitate a direct comparison of our measurements of the FM and CO/OO/AF phases in LPCMO, we have plotted in Fig. 3(d) the magnetization, determined by dividing each image, pixel by pixel, by the coldest in its cycle for three different cooling-warming cycles. We emphasize that these measurements were

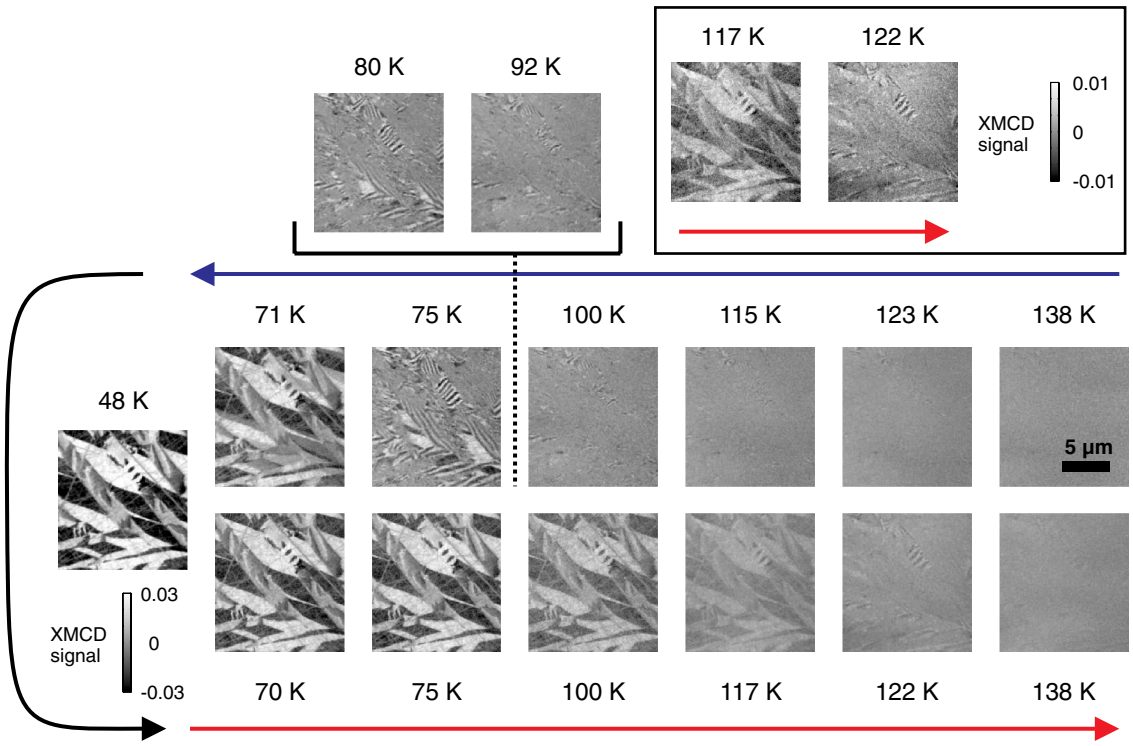

FIG. 2 (color online). PEEM data: XMCD images taken while cooling and warming the sample. Inset: The two images on either side of T_C, warming, with enhanced contrast to highlight the changes in the domain pattern across T_C. 48 K was the lowest temperature that we could achieve.

performed in zero applied magnetic field, which is critical for a compound where a magnetic field can shift the balance from one ordered phase to another. It is clear from Fig. 2 that the transition into the FM phase occurs over a large temperature range, with FM and non-FM regions coexisting, so when the magnetic moment jumps, it does not immediately line up with the warming curve. For $T \ll T_C$, the magnetization decreases linearly with increasing temperature rather than saturating quickly.

All of the unusual phenomena we observed can be attributed to the glassy nature of the CO/OO/AF, similar to the glassy polarons in bilayered $La_{2-2x}Sr_{1+2x}Mn_2O_7$ and in $La_{0.7}Ca_{0.3}MnO_3$. In LPCMO, the striped structure of the FM domains that are present around 80 K cooling (Fig. 2) indicate that the environment there is different from that well below T_C, likely due to remaining lattice strain. When the sample is cooled further, the FM phase becomes energetically more favorable, so it eventually encompasses almost the whole sample. On warming, the striped FM domain structure is not present, as is clear in the inset to Fig. 2. The reason for this is that the FM phase maintains control over the lattice until it disappears at T_C. The unconventional behavior of the correlation length of the CO/OO/AF regions above T_C (Fig. 3(b)) is also consistent with a glass transition. On cooling, the lattice distortions freeze at T_g, locking in the domain sizes. Below T_C, the majority of the charge carriers are itinerant, allowing much larger CO/OO/AF domains to form at T_C on warming. As the sample is warmed further, the average domain size rises until T_g; this is due to the the smaller CO/OO/AF domains melting first, as is common in glasses [14]. When the sample is warmed through T_C and then cooled, the CO/OO/AF domains stay the same size, as they do during a traditional cooling scan, but are able to persist to a lower temperature.

Below T_C, the CO/OO/AF and FM phases coexist. The slow change in q of the CO/OO/AF combined with the unusual linear temperature dependence of XMCD amplitude suggests that there is a battle going on between the two phases. As the sample is cooled, the FM phase works its way into the regions of accommodation strain, forcing them to relax, and in turn reducing the overall lattice distortions within the CO/OO/AF. That the correlation length is steady means that the boundaries of the CO/OO/AF must be frozen, and this is the reason that phase separation exists. Previous measurements of compounds in the LPCMO series (including $y = 0.275$) have shown a kinetic arrest at 20 K [15]. This can be interpreted as the lattice completely freezing: the accommodation strain no longer relaxes to maintain some sort of equilibrium between the FM and CO/OO/AF phases.

One point of interest is that the the domain sizes of the different types of order differ by an order of magnitude: the CO/OO/AF correlation lengths are less that 150 nm, while

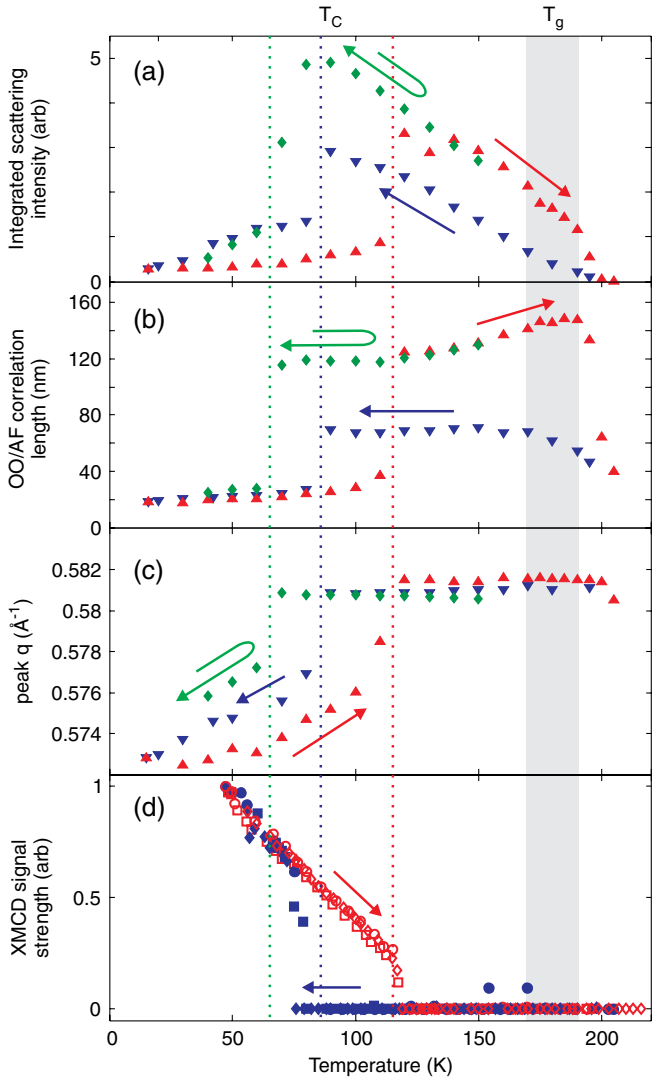

FIG. 3 (color online). RSXS data: (a) Integrated RSXS intensity, (b) correlation length, and (c) q of the CO/OO/AF domains. (▲) warming; (▼) cooling from room temperature; (◆) cooling, after warming from 32 K to 150 K. (d) Magnetization determined from XMCD, normalized to the coldest image. Different symbols represent different cooling-warming cycles. Squares represent the images shown in Fig. 2. Dotted vertical lines represent T_C as determined by the RSXS measurements; it is different for each of the three measurement schemes. The gray band represents T_g, as the glass transition does not have a sharp onset.

the FM domains can grow to a few microns. The former are similar in size to those in $Pr_{1-x}Ca_xMnO_3$, which is significantly more favorable to CO/OO/AF and has no FM order [12], implying that there is an intrinsic limit to their size. Based on our findings, this limit comes from the glassy nature of their associated lattice distortions, in a similar manner to the glassy martensite in $Ti_{50-x}Ni_{50+x}$ [16]. As the FM phase introduces no lattice distortions, the size of FM domains is not limited by the same phenomenon.

To summarize, our results imply that the glassy nature of either single polarons or CO/OO/AF plays a critical role in phase separation and in the nature of the transition into the FM phase in manganites. Furthermore, there are many other compounds in the manganite series with a CO/OO/AF ground state, and they show strong CMR: a magnetic field of a few tesla reduces their resistivity by orders of magnitude [17]. The application of a field induces the FM state, but the details of the phase transition are unknown. In LPCMO, the phase transition from CO/OO/AF to FM occurs at zero field, so our measurements could indicate how the phase transition occurs in compounds where it is field-induced and the nature of CO/OO/AF in compounds without a FM ground state. A slow transition from glassy CO/OO/AF to strained FM order to unstrained FM order would explain the large change in resistivity and field required for it. In the FM phase, there are still regions of collective lattice distortions that clearly suppress the FM order and result in large CMR even in manganites with an FM ground state. Overall, our results show that the glassy nature of superlattice order is an integral part of phase separation and CMR.

Work at SIMES, the ALS, and Rutgers is supported by the U.S. Department of Energy, Office of Basic Energy Sciences, Division of Materials Sciences and Engineering, under Contracts No. DE-AC02-76SF00515, No. DE-AC02-05CH11231, and No. DE-FG02-07ER46382, respectively. M. A. H. acknowledges support from NSERC, Canada.

*hossain@slac.stanford.edu

[1] E. Dagotto, T. Hotta, and A. Moreo, Phys. Rep. **344**, 1 (2001).
[2] Y. Tokura, Rep. Prog. Phys. **69**, 797 (2006).
[3] J. Tao, D. Niebieskikwiat, M. Varela, W. Luo, M. A. Schofield, Y. Zhu, M. B. Salamon, J. M. Zuo, S. T. Pantelides, and S. J. Pennycook, Phys. Rev. Lett. **103**, 097202 (2009).
[4] D. N. Argyriou, U. Ruett, C. P. Adams, J. W. Lynn, and J. F. Mitchell, New J. Phys. **6**, 195 (2004).
[5] C. P. Adams, J. W. Lynn, Y. M. Mukovskii, A. A. Arsenov, and D. A. Shulyatev, Phys. Rev. Lett. **85**, 3954 (2000); P. Dai, J. A. Fernandez-Baca, N. Wakabayashi, E. W. Plummer, Y. Tomioka, and Y. Tokura, Phys. Rev. Lett. **85**, 2553 (2000).
[6] J. W. Lynn, D. N. Argyriou, Y. Ren, Y. Chen, Y. M. Mukovskii, and D. A. Shulyatev, Phys. Rev. B **76**, 014437 (2007).
[7] D. N. Argyriou, J. W. Lynn, R. Osborn, B. Campbell, J. F. Mitchell, U. Ruett, H. N. Bordallo, A. Wildes, and C. D. Ling, Phys. Rev. Lett. **89**, 036401 (2002).
[8] M. Uehara, S. Mori, C. H. Chen, and S. W. Cheong, Nature (London) **399**, 560 (1999).
[9] V. Podzorov, B. G. Kim, V. Kiryukhin, M. E. Gershenson, and S.-W. Cheong, Phys. Rev. B **64**, 140406 (2001).

[10] K. J. Thomas, J. P. Hill, S. Grenier, Y. J. Kim, P. Abbamonte, L. Venema, A. Rusydi, Y. Tomioka, Y. Tokura, D. F. McMorrow, G. Sawatzky, and M. van Veenendaal, Phys. Rev. Lett. **92**, 237204 (2004).

[11] U. Staub, M. García-Fernández, Y. Bodenthin, V. Scagnoli, R. A. DeSouza, M. Garganourakis, E. Pomjakushina, and K. Conder, Phys. Rev. B **79**, 224419 (2009).

[12] S. Y. Zhou, Y. Zhu, M. C. Langner, Y.-D. Chuang, P. Yu, W. L. Yang, A. G. Cruz Gonzalez, N. Tahir, M. Rini, Y.-H. Chu, R. Ramesh, D.-H. Lee, Y. Tomioka, Y. Tokura, Z. Hussain, and R. W. Schoenlein, Phys. Rev. Lett. **106**, 186404 (2011).

[13] To compensate for the imperfect overlap of the left and right circularly polarized beams, we averaged all of our XMCD images that do not show magnetic domains to generate a background, which we subtracted from all of the images shown in this Letter.

[14] Y. Wang, X. Ren, K. Otsuka, and A. Saxena, Phys. Rev. B **76**, 132201 (2007).

[15] P. A. Sharma, S. B. Kim, T. Y. Koo, S. Guha, and S.-W. Cheong, Phys. Rev. B **71**, 224416 (2005); P. A. Sharma, S. El-Khatib, I. Mihut, J. B. Betts, A. Migliori, S. B. Kim, S. Guha, and S.-W. Cheong, Phys. Rev. B **78**, 134205 (2008); M. H. Phan, M. B. Morales, N. S. Bingham, H. Srikanth, C. L. Zhang, and S.-W. Cheong, Phys. Rev. B **81**, 094413 (2010); W. Wu, C. Israel, N. Hur, S. Park, S.-W. Cheong, and A. de Lozanne, Nature Mater. **5**, 881 (2006).

[16] S. Sarkar, X. Ren, and K. Otsuka, Phys. Rev. Lett. **95**, 205702 (2005).

[17] Y. Tomioka, A. Asamitsu, H. Kuwahara, Y. Moritomo, and Y. Tokura, Phys. Rev. B **53**, R1689 (1996).